

Review

Guidelines for Determining the Initial Shape and Specifications of High-Speed AFPM Based on Recent Research

Jae-Beom Kang ^{1,2} , Ji-Young Lee ^{1,2,*}  and Ji-Heon Lee ^{1,3} 

¹ Air Mobility Electric-Motor & Drive Research Team, Korea Electrotechnology Research Institute (KERI), Changwon 51543, Korea

² Electric Energy Conversion Engineering, University of Science and Technology (UST), Daejeon 34113, Korea

³ Mechanical Engineering, Pusan National University (PNU), Pusan 46241, Korea

* Correspondence: jylee@keri.re.kr

Abstract: This paper presents guidelines for determining the initial shape and specifications of a high-speed axial-flux permanent-magnet (AFPM) machine in a hybrid-electric propulsion system in two steps based on previous studies and product review results related to high-speed AFPMs. In the first step, three characteristics to be considered when designing AFPMs were classified as: electromagnetic, thermal, and mechanical. Then, the factors that should be considered in the design process to satisfy each characteristic were organized. In the second step, “the speed–output power” relationship was defined to predict the limits of applying AFPMs to high-speed applications, allowing an estimation of the limits of the speed range that can be used within the proposed output power.

Keywords: axial-flux permanent-magnet machine (AFPM); high-speed electric machine; air mobility; design key issues; dynamic performance limit



Citation: Kang, J.-B.; Lee, J.-Y.; Lee, J.-H. Guidelines for Determining the Initial Shape and Specifications of High-Speed AFPM Based on Recent Research. *Energies* **2022**, *15*, 6099. <https://doi.org/10.3390/en15166099>

Academic Editor: Federico Barrero

Received: 1 July 2022

Accepted: 17 August 2022

Published: 22 August 2022

Publisher's Note: MDPI stays neutral with regard to jurisdictional claims in published maps and institutional affiliations.



Copyright: © 2022 by the authors. Licensee MDPI, Basel, Switzerland. This article is an open access article distributed under the terms and conditions of the Creative Commons Attribution (CC BY) license (<https://creativecommons.org/licenses/by/4.0/>).

1. Introduction

Recently, since the international interest in resolving global warming issues has increased, the United Nations has set requirements for industries that emit a lot of carbon, one of the main causes of global warming, to reduce their carbon emissions. Accordingly, many researchers have been actively conducting research to satisfy this requirement [1–3].

The transportation industry is one of the highest carbon-emitting industries. Accordingly, to reduce carbon emissions, the transportation industry is actively trying to utilize electric power instead of fuel power for the propulsion systems of various vehicles [1,3,4].

Among the land, sea, and air vehicles used in the transportation industry, electric power propulsion systems for land vehicles have been commercialized beyond the research and development (R&D) stage, but the electric power propulsion systems for sea and air vehicles are still in the R&D stage. In particular, R&D and the commercialization of electric power propulsion systems for air vehicles are progressing at a slower speed compared with other vehicles because the required stability and power density levels are relatively high compared with other vehicles [5,6].

Engines and generators are the main power sources for hybrid electric propulsion systems used in air vehicles. Recently, their operating speeds have been gradually increased to achieve high power density [7–9]. In addition, to increase space utilization, a flat-type generator with a diameter similar to that of an engine and a short axial length is required [7].

As generators that suit these requirements, axial-flux permanent-magnet (AFPM) machines have been attracting much attention. An AFPM is a permanent magnet machine in which the rotor and stator are arranged perpendicular to the rotation axis so that the magnetic flux direction passing through the air gap is the same as the axial direction [8]. Therefore, it is known that the AFPM has a higher torque per unit area of the rotor and a shorter axial length than the radial-flux permanent-magnet (RFPM) machines [10–12]. However, there are also some disadvantages due to the structural characteristics of AFPMs.

For example, due to the large diameter, a strong centrifugal force is applied to the rotor, which makes the rotor easy to deform, and the permanent magnets are easy to break or detach from the rotor. More details are provided in a later section. Although many papers discussed the superiority of the electromagnetic characteristics of AFPM machines, there are only a few cases in which AFPM machines were commercialized. This is because, in order to commercialize AFPM machines, not only the electromagnetic characteristics but also the thermal and mechanical characteristics required by air transport systems must be satisfied [13].

In this paper, based on the papers that manufactured the AFPM and presented the test results, guidelines for determining the initial shapes and specifications of the AFPM machines used in high-speed generators are presented in two steps.

In the first step, the three characteristics to consider when designing an AFPM machine as a high-speed generator were categorized as: electromagnetic, thermal, and mechanical characteristics. Then, to satisfy these characteristics, the key issues to consider in the design process are summarized in Sections 2–5. First, Section 2 briefly describes the types, shapes, and characteristics of AFPM topologies to help understand AFPM machines. In Section 3, the standard speed for determining the high-speed region is defined, the papers on the AFPM products operating in the high-speed region are explored, and the topology of AFPM machines are arranged and presented. Section 4 reviews the papers investigated in Section 3 and presents key issues that occur at high speed by classifying them as three characteristics: electromagnetic, thermal, and mechanical. Section 5 presents some cases from the papers which deal with the key issues discussed in Section 4.

In the second step, the “speed–output power” characteristic was defined and analyzed to predict the limit when applying the AFPM to high-speed applications. This step is covered in Section 6, which also defines a function that determines the limit of the “speed–output power” of the high-speed AFPM machines presented in the collected literature. Through this definition, it is possible to estimate the limit of the speed range that can operate within the required output power range. Additionally, by comparing and analyzing the speed–output power limit curve of the AFPM and the speed–output power limit curve of the RFPM, the advantages and disadvantages were identified, and the limits of the AFPM were presented more objectively.

2. AFPM Topologies

In this section, the shape and characteristics of the AFPM topology are briefly explained to help understand AFPMs.

As shown in Figure 1, the topology of the AFPM can be classified into four types according to the rotor–stator combination: single-stator single-rotor (SSSR), double-stator single-rotor (DSSR), single-stator double-rotor (SSDR), and multistage AFPM [12,14].

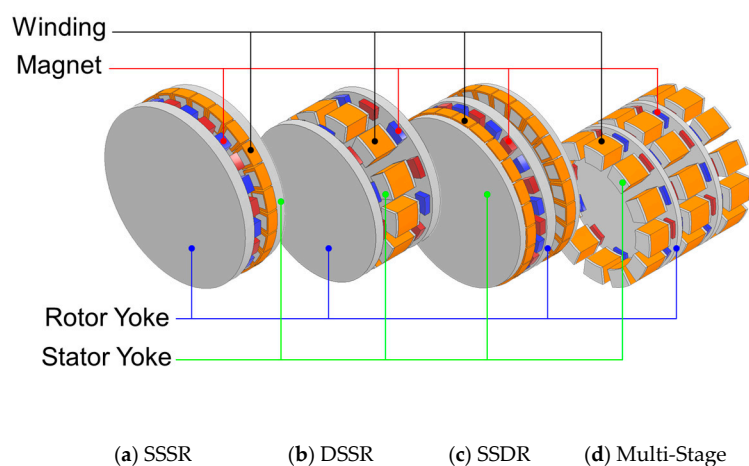


Figure 1. Shape of the AFPM topology.

SSSR is the most basic structure of the AFPM, and it is composed of one rotor and one stator, as shown in Figure 1a. This topology is relatively easy to manufacture and has the thinnest structure among AFPM topologies [15]. Thus, it is often used for driving small fans. However, it is difficult to maintain the gap between the rotor and stator due to the strong axial attraction force. To solve this problem, it is necessary to consider using thrust bearings instead of ball bearings or using a coreless stator.

DSSR is a structure composed of two stators and one rotor, as shown in Figure 1b. In this topology, the attraction force is balanced because the rotor is between the two stators. Therefore, unlike other AFPM topologies, this topology does not require mechanical measures to withstand axial attraction forces [16]. However, since there are two stators through which current flows, the length in the axial direction is relatively long, making it difficult to implement the flat-type generator, which is characteristic of the AFPM.

SSDR is a structure composed of one stator and two rotors, as shown in Figure 1c. Since this topology has two rotors, it has more magnets than the previous two topologies. As a result, relatively high power can be achieved compared with the topologies that only use one rotor. In addition, this topology can eliminate the yoke of the stator depending on how the poles of the permanent magnets attached to the two rotors are arranged, thereby reducing the loss and weight compared with other topologies [16].

Multistage AFPM is a structure composed of two or more stators and rotors, as shown in Figure 1d. This topology can produce the highest power among AFPM topologies [8]. However, its disadvantage is that the axial length is long, making it unsuitable for the purpose of this paper: determining the design specifications of disk-type generators. Therefore, starting from the next section, this paper does not discuss this topology.

3. Definition of High-Speed AFPMs and Characteristics of The AFPM Topology

To review high-speed AFPMs (HSAFPMs), “high-speed” must be defined. Many papers dealing with high-speed electric machines define whether a machine is a high-speed machine or not based on its rotational speed [10,17,18]. However, there are papers that define high-speed machines based on linear speed [19]. This is because mechanical analyses are required not only for high-speed defined machines (due to their small rotor diameter and high rotational speed) but also for the machines with low rotational speeds but large rotor diameters. In ref. [19], the authors defined whether a machine is high speed or not based on a linear speed that not only reflects the rotational speed of the machine, but also its structural characteristics, such as the rotor diameter. The linear speed definition is described by Equation (1):

$$V = r \frac{2\pi}{60} N \quad (1)$$

where r denotes the rotor’s radius, and N denotes the rotor’s rotational speed.

Within the same machine volume, the AFPM has a structural characteristic where the rotor diameter is relatively larger than that of an RFPM. Thus, the AFPM may have a structural problem due to its large linear velocity even if the rotational speed is slow. Therefore, in this paper, whether the AFPM is high speed or not is defined based on the linear speed.

To determine the standard value defining the high speed based on the linear speed, the relationship between the rotational speed and linear speed was summarized, as shown in Figure 2, by calculating the linear speed of the RFPM prototypes presented in ref. [20–29], which defined high speed based on the rotational speed. It can be confirmed that the linear speed of an RFPM with a rotational speed of ~10,000 rpm or more is 50 m/s or more. Thus, in this paper, the linear speed of 50 m/s is defined as a standard speed for an HSAFPM.

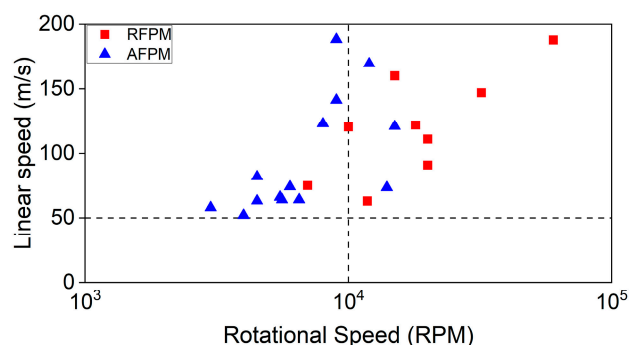


Figure 2. Linear speed–rotational speed relationship of RFPM and AFPM.

The papers that manufactured and tested AFPM prototypes with a linear speed of 50 m/s or more were collected and listed in Table 1, which is arranged in descending order based on the linear speed, and the main characteristics, such as topology, output power, cooling method, and $\text{RPM}\sqrt{\text{kW}}$, are also arranged. $\text{RPM}\sqrt{\text{kW}}$ is the figure of merits that evaluates the dynamic performance of machines. Additionally, this is discussed in detail in Section 6. To more intuitively analyze the main characteristics arranged in the table, the main characteristics are shown in Figure 2.

Table 1. Summary table of references related to HSAFPM.

Reference No.	Topology	Power (kW)	N (krpm)	V (m/s)	$\text{RPM}\sqrt{\text{kW}}$	Cooling Method
[30]	SSSR	0.1	45	330	14,230	-
[10]	SSDR	50	9	188	63,640	Oil cooling
[31]	DSSR	90	12	170	113,842	Water cooling
[32]	DSSR	45	12	170	80,498	Water cooling
[33]	DSSR	85	9	141	82,976	Water cooling
[34]	SSDR	60	8	123	62,000	-
[35]	SSDR	20	15	121	67,082	-
[36]	SSDR	210	4.5	82	65,211	Air + water cooling
[37]	SSSR	15	6	74	23,238	Air cooling
[38]	SSDR	0.4	14	73	8854	-
[39]	SSDR	62	5.5	66	43,310	Air + water cooling
[40]	DSSR	36	5.6	64	33,600	Water cooling
[41]	SSDR	30	6.5	64	35,602	Air + water cooling
[42]	SSDR	107	4.5	63	46,548	Air + water cooling
[43]	SSDR	70	3	58	25,100	-
[44]	SSDR	60	4	52	30,984	Water cooling

Figure 2 organizes the relationship between the rotational speed and linear speed of high-speed RFPM machines. By indicating the relationship between the rotational speed and linear speed of the AFPM products listed in Table 1, the difference between the relative speed ranges of the RFPM and AFPM can be observed. That is, in terms of the linear speed, both the RFPM and AFPM are equally distributed between 50 m/s and 200 m/s. However, the RFPM is mostly located on the right side of the graph, showing a rotational speed of 10,000 RPM or more. Conversely, the AFPM, which has a relatively large rotor diameter, is mostly located on the left side of the graph, showing a rotational speed of 10,000 RPM or less.

4. Key Issues in HSAFPM Design

In this section, by analyzing the HSAFPM-related papers and products summarized in Table 1, the key issues to be considered when designing the HSAFPM are presented by classifying them based on three characteristics: electromagnetic, thermal, and mechanical. Since the solution of the design process presented in the literature for each proposed key issue is summarized in Section 5, this section focuses on defining the key issues to understand the solution.

4.1. Electromagnetic Key Issues

The electromagnetic key issues to consider when designing the HSAFPM are the core losses and the eddy current losses of the permanent magnet. The magnitude of these losses is proportional to the frequency and output power, and the larger these losses, the higher the temperature of the machine or the lower the efficiency of the machine [38,44]. In addition, when a Nd-based PM vulnerable to high temperature is used to obtain a high power density, the PM may be demagnetized or oxidized by heat due to losses. Therefore, it is essential to reduce these two losses when designing the HSAFPM.

4.1.1. Core Losses

The core losses can be classified into several terms. However, most fundamentally, they can be explained by classifying them as two terms: hysteresis loss and eddy current loss [45]. Additionally, core losses are defined by Equation (2) [46]:

$$P_h + P_e = k_h f B^n + k_e h^2 f^2 B^2 \quad (2)$$

where k_h is a constant that depends on the material type and dimensions, f denotes the electrical frequency, B is the flux density amplitude within the material, n is a material-dependent exponent that is usually between 1.5 and 2.5, h is the material thickness, and k_e is a material-dependent constant.

The hysteresis loss, which is the left term of Equation (2), is caused by the magnetomotive force (MMF) applied to the iron core, and the magnitude of this loss is proportional to the inner area of the hysteresis loop.

The eddy current loss, which is the right term of Equation (2), is caused by the change in the MMF applied to the iron core, and the magnitude of this loss is proportional to the length of the current path flowing in the iron core.

4.1.2. Eddy Current Loss of the Permanent Magnet (PM)

The eddy current loss in the PM can be calculated by the Joule loss formula using the eddy current flowing through the PM and the resistance determined by the eddy current path. The definition of the Joule loss is explained by Equation (3) [47]:

$$P_{em} = I^2 R_{PM} R_{PM} = \rho_{PM} \frac{L_{PM}}{A_{PM}} \quad (3)$$

where I is the eddy current flowing through the PM, R_{PM} is the resistance of the eddy current path of the PM, ρ_{PM} is the electrical resistivity of PM, L_{PM} is the length of the eddy current path of the PM, and A_{PM} is the cross-sectional area of the PM.

4.2. Thermal Key Issues

The mechanical and electromagnetic losses in electric machines generate heat, which reduces the efficiency of electric machines. Thus, to increase this efficiency, it is necessary to reduce the mechanical and electromagnetic losses or to quickly remove the generated heat inside the machines through cooling.

The mechanical losses in the HSAFPM are very low compared with the electromagnetic losses, or they can be due to the bearing or assembly characteristics. Thus, they are not discussed in this section. The main heat source, electromagnetic loss, is dealt with separately

in the “Electromagnetic Key Issues” section, and the “Thermal Key Issues” section only deals with cooling.

Cooling utilizes a heat transfer mechanism. Therefore, here, the three basic laws of heat transfer, conduction, convection, and radiation, are summarized.

4.2.1. Conduction

Through heat conduction, the heat present in a solid is transferred from the high-temperature side to the low-temperature side. “Fourier’s law of heat conduction” is defined by Equation (4):

$$Q_{CD} = kA_{sur} \frac{\Delta T}{\Delta x} \quad (4)$$

where k is a material’s conductivity, A_{sur} is the cross-sectional surface area, ΔT is the temperature difference between the ends, and Δx is the distance between the ends.

4.2.2. Convection

Through heat convection, heat is transferred through the movement of a fluid, and “Newton’s cooling law” for convection is defined by Equation (5):

$$Q_{CV} = h_{cv}A_{cont}\Delta T \quad (5)$$

where h_{cv} is the convection heat transfer coefficient, A_{cont} is the contact area between the solid and fluid, and ΔT is the temperature difference.

4.2.3. Radiation

Through heat radiation, heat is directly transferred from a hot object to the surrounding air through electromagnetic waves. The “Stefan–Boltzmann law” for radiation is defined by Equation (6):

$$Q_{RA} = \varepsilon\sigma A_{RA} (T_s^4 - T_a^4) \quad (6)$$

where ε is the emissivity, σ is Stefan’s constant, A_{RA} is the radiating area, T_s is the material temperature, and T_a is the temperature of the surroundings.

As shown in Equations (4)–(6), the heat transfer mechanism through conduction, convection, and radiation is proportional to the temperature difference between the two materials. It can also be seen that heat conduction is proportional to the cross-sectional area of the material and that heat convection and radiation are proportional to the surface area of the material. Therefore, to increase the cooling efficiency, it is necessary to use the coolant at a much lower temperature than the internal temperature of the machine and increase the cross-sectional area and surface area of the internal parts of the machine. However, if the temperature difference between the coolant and the internal components is too large, thermal deformations may occur in the internal components. Therefore, in the high-speed machines that generate large losses, an appropriate cooling method must be applied, and the use of thermal analyses is essential.

4.3. Mechanical Key Issues

The key mechanical issues to consider when designing the HSAFPM are the attractive and centrifugal forces. The definition of each force and its effect on the HSAFPM are explained below.

4.3.1. Attractive Force

The attractive force is a force acting between two objects made of a ferromagnetic material, and it acts in the direction of their attraction to each other. In the AFPM, it occurs between the PM attached to the rotor and the stator or between the two rotors. Therefore, if the magnitude of this force is large, the PM may fall from the rotor core. Additionally, this force makes it difficult to keep the distance between the rotor and stator constant, and it can cause deformations in the rotor or stator. Furthermore, an axial force is applied to the

bearings supporting the rotor and stator, which may cause problems, such as vibrations. As a result, when designing the HSAFPM, it is necessary to design the structure considering the attractive force.

4.3.2. Centrifugal Force

The centrifugal force is defined as the inertial force that appears in a rotating object, and the direction of this force is the radial direction of the rotor. The PMs of the AFPM are generally arranged in the circumferential direction of the rotor core's surface and are adhered with an adhesive substance or inserted inside. The centrifugal force acts as a radial tensile force on the PM. The permissible tensile strength of the PM is ~10 times lower than the compressive strength. Thus, if the centrifugal force is large, a problem may occur with regard to the stability of the PM.

5. Solutions for the Key Issues in HSAFPM Design

This section describes the investigations and analyses of the representative literature that provided solutions to the key issues classified in Section 4: electromagnetic, thermal, and mechanical characteristics.

5.1. Solutions for the Electromagnetic Key Issues

5.1.1. Hysteresis Core Loss

Z Wang et al. [38] proposed a method for reducing the hysteresis loss by fabricating stator cores using amorphous magnetic materials (AMMs). Unlike crystalline materials, which have a regular arrangement of atoms, AMMs have relatively short hysteresis loops due to their irregular arrangement of atoms. The authors of this paper compared the hysteresis losses of Si-Fe, soft magnetic composites, and Fe-AMM, and confirmed that Fe-AMM has the lowest hysteresis loss. Based on the comparison results, the authors fabricated the HSAFPM using a stator core made from an AMM material and showed that the efficiency of the fabricated machine increased by using a performance test.

5.1.2. Eddy Current Loss of the Core

The authors of [9] used a coreless SSDR to reduce the eddy current loss. Coreless (ironless) stators have no cores or are made of nonmagnetic materials. Thus, magnetic flux paths are either not created or are very short. Therefore, there is almost no eddy current loss in the stator. However, if a coreless stator is used, the leakage of the magnetic flux flowing from the PM to the stator is large. Thus, its disadvantage is that it may lead to a lower power density than that of a cored SSDR. The authors of [48] used a wound core stator to reduce the eddy current losses in an SSDR AFPM. Unlike stacked cores, which are manufactured by stacking steel sheets, as shown in Figure 3a, wound cores are manufactured by rolling steel sheets, as shown in Figure 3b. In the AFPM, the magnetic flux flow is in the axial direction. Therefore, a wound core that is laminated in a direction perpendicular to the magnetic flux, i.e., a radial direction, is more advantageous than a stacked core that is laminated in the axial direction.

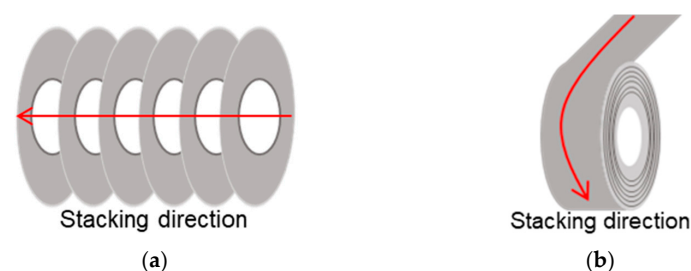


Figure 3. Stator core types. (a) is a stacked core, which refers to a core in which steel sheets are stacked in the vertical direction of the axis; (b) is a wound core, which refers to a core in which steel sheets are stacked in the radial direction of the axis.

5.1.3. Eddy Current Loss of the PM

The authors of [16,49] reduced the eddy current loss by separating the PM in the radial direction. With a separated PM, the eddy current loss is reduced because the eddy current path on the surface of the PM is shortened. Furthermore, in ref. [16], the rotor heat distribution, which varies according to the number of separated PMs, was comparatively analyzed using the lumped parameter method and finite element method. The authors proved that the method of separating the magnet significantly reduces the eddy current loss and that it is quite effective in reducing the temperature of the PM.

However, when PMs are segmented, as proposed in the above works, a repulsive force is generated between the segmented magnets. Therefore, if a permanent magnet is separated excessively to reduce the eddy current loss, it is difficult to fix it to the rotor due to the repulsive force generated between the separated magnets. Thus, the method of reducing the eddy current loss by separating permanent magnets must consider the repulsive force generated between the separated magnets.

5.2. Solutions for the Thermal Key Issues

All cooling methods of the HSAFPM prototypes listed in Table 1 are schematically shown in Figure 4. Of the 16 prototypes, 27.5% have an unknown cooling method, 5.5% use air cooling, and the remaining 67% use liquid cooling. The main advantage of air cooling is its simple structure. However, its cooling performance is inferior to that of water cooling. Although liquid cooling has a relatively good cooling performance, it makes it difficult to form a flow path and increases the machine's weight.

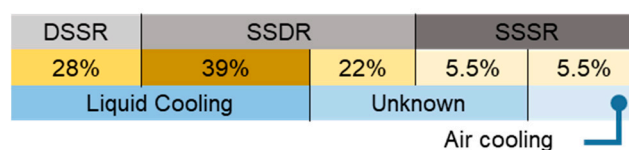


Figure 4. All cooling methods of HSAFPM prototypes listed in Table 1.

Among the various liquid cooling methods with good cooling performance, three design cases for a new cooling method applied to the HSAFPM are herein introduced.

As a first case, Zhouan Zhang et al. [9] proposed an ironless stator structure with excellent cooling performance. The proposed stator structure consists of windings, an epoxy support engraved with a waterway, and an epoxy sheet. First, the authors fixed the front and back sides of the windings with epoxy supports to increase the strength and rigidity of the windings. Thereafter, a cavity was formed in the stator by covering both sides of the epoxy support with an epoxy sheet, where the cavity serves as the entrance or exit to the waterway. Therefore, this structure has good cooling performance because the coolant flows very close to the stator.

As a second case, Wei Le et al. [44] proposed a cooling method that combines a flat heat pipe and housing through which coolant flows. The flat heat pipe absorbs the external heat and vaporizes the fluid inside the pipe. The authors installed flat heat pipes between each stator tooth so that they absorb the heat inside the stator. As the flat heat pipes absorb heat, the fluid flowing inside the pipe is vaporized and expanded. Then, the expanded hot vapor moves toward the housing and is condensed through cooling. The authors performed thermal property experiments and computational fluid dynamics (CFD) analyses to confirm the performance of the proposed cooling method. However, they did not demonstrate how this method is superior to the methods that only use housing through which coolant flows.

As a last case, [50] proposed a cooling method by inserting a copper tube through which cooling water flows into a yokeless stator. The method proposed by [50] can quickly dissipate the generated heat in the winding by attaching the copper tube to the stator winding. Moreover, the empty space inside the stator is filled with an epoxy material with high thermal conductivity to reduce thermal resistance and increase stability and rigidity.

The authors of [50] analyzed the performance of the proposed cooling structure through CFD in the same way as in ref. [44]. However, this study did not analyze how superior the performance of the proposed cooling method was compared with that of the conventional cooling method.

5.3. Solutions for the Mechanical Key Issues

5.3.1. Attractive Force

Junquan Lai et al. [16] proposed a method in which a rotor cover is attached to the rotor to protect the permanent magnet from the attractive force between the rotor and the stator core in the DSSR topology. The authors of [16] calculated the attractive force between the rotor and stator and calculated the deformations of the rotor and rotor cover due to the attractive force through FEM. Through these calculations, the structural stability of this method was verified by proving that the deformations of the rotor and rotor core are within the allowable ranges.

B. Zhang et al. [50] reduced the influence of the attractive force through proper bearing selection and an adhesive performance test in the SSDR topology. First, the authors firmly fixed the rotor with two fixed bearings (spindle bearings) that were fixed in the axial direction and one floating bearing (grooved ball bearing) that was fixed in the radial direction. The performance of the adhesive used to attach the permanent magnet to the rotor core was tested to confirm the possibility of the PM's detachment by the attractive force.

Unlike [50], which used an adhesive to fix the PM, Zhouuran Zhang et al. [10] fixed the PM through a special PM shape and slot pins, as shown in Figure 5. The authors fixed the magnet so it does not move in the axial direction by inserting a slot pin into the slot opening of the PM.

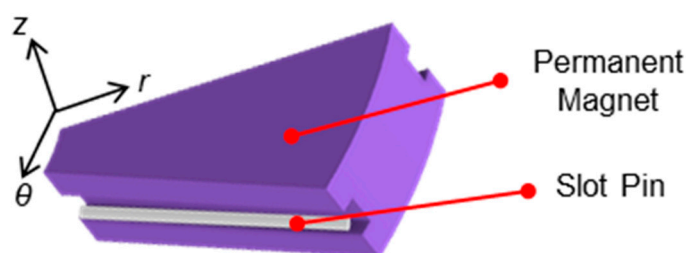


Figure 5. Example of magnet and slot pin [10].

5.3.2. Centrifugal Force

Because the centrifugal force causes the same problem in a high-speed RFPM as in a high-speed AFPM, many studies have relatively been conducted as compared with other key issues. As a result, methods for solving the above problems have been proposed in many papers, and the proposed methods can be divided into two methods.

The first method is to install a retaining ring on the outer surface of the PM and apply compressive stress to the PM, subjecting it to tensile stress due to the centrifugal force. The advantages of this method are the easy manufacturing process of the rotor and that it is low cost, as there is no need to manufacture a rotor with a special structure. However, if the retaining ring applies too much compressive stress to the PM, the PM may be damaged. Conversely, if the compressive stress that is applied is too weak, the tensile stress cannot be reduced.

The second method is to insert a PM inside the rotor [30]. This method easily prevents the PM from being destroyed, as the PM is inside the rotor. However, its disadvantage is that it is difficult to manufacture the rotor compared with the previous method. Thus, the manufacturing cost is high [30].

6. Dynamic Performance Limit Curve of AFPM

6.1. Dynamic Performance Limit Curve of HSAFPM

This section describes the second step to consider when designing an HSAFPM. In particular, it defines and analyzes the “speed–output power” relationship to predict the speed limit when the AFPM is applied to high-speed applications.

The authors of [51] presented a figure of merit indicating the speed–power (dynamic performance) limit of a rotating machine from a mechanical point of view. The proposed figure of merit is $\text{RPM}\sqrt{\text{kW}}$, and it is defined by Equation (7):

$$\text{RPM}\sqrt{\text{kW}} = N \times \sqrt{P} \quad (7)$$

where N is the rotational speed (rpm) of the machine, and P is the output power (kW) of the machine.

In ref. [4,51], the authors presented dynamic performance limit curves for each topology of electric machines. However, for PM machines, only dynamic performance limit curves for the detailed topologies of the RFPM, and not for the AFPM, were presented. Therefore, this paper presents the dynamic performance limit curve of the HSAFPM with reference to [4,51].

To find the function for the dynamic performance limit curve of the HSAFPM, the maximum speed and maximum output power values of the 16 prototypes in Table 1 were calculated by substituting them into Equation (7). Among the AFPM prototypes, [31] has the largest $\text{RPM}\sqrt{\text{kW}}$ value. Thus, the function of the dynamic performance limit curve becomes $\text{RPM}\sqrt{\text{kW}} = 1.14 \times 10^5$. In Figure 6, it can be seen that the speed–output power points of the 16 prototypes in Table 1 are located within the defined dynamic performance limit curve.

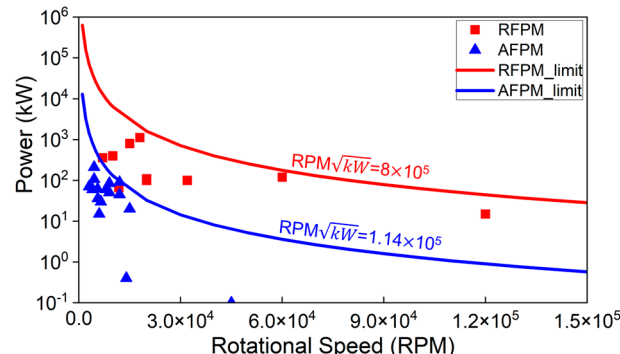


Figure 6. Dynamic performance limit curve of HSAFPM and HSRFPM.

To objectively evaluate the dynamic performance limit curve of the HSAFPM, a relative comparison was performed. In other words, to compare the dynamic performances of the AFPM and RFPM, the dynamic performance curve of the RFPM was also reviewed. In ref. [4], the dynamic performance limit curve of the RFPM was presented as $\text{RPM}\sqrt{\text{kW}} = 8 \times 10^5$. However, it was necessary to check whether this limit curve is still valid since it was published in 2014. Therefore, we first checked whether the dynamic performance limit curve of the RFPM presented in ref. [4] is valid by investigating the high-speed RFPM (HSRFPM) papers conducted since ref. [4] was published. Afterward, $\text{RPM}\sqrt{\text{kW}}$ was calculated and listed in Table 2. Among the 10 prototypes investigated, the $\text{RPM}\sqrt{\text{kW}}$ value did not exceed the dynamic performance limit of the RFPM presented in ref. [4]. Therefore, it was confirmed that the dynamic performance limit curve of the RFPM presented in ref. [4] is still valid.

Table 2. RPM \sqrt{kW} of HSRFPM.

Reference No.	Topology	Power (kW)	N (krpm)	RPM \sqrt{kW}
[18]	RingPM	120	60	657,267
[21]	SPM	1120	18	602,395
[27]	SPM	15	120	464,758
[25]	SPM	800	15	424,264
[20]	SPM	100	32	320,000
[22]	RingPM	110	20	209,762
[23]	SPM	100	20	200,000
[24]	SPM	400	10	200,000
[19]	SPM	360	7	132,816
[26]	SPM	66.6	11.8	96,298

Figure 6 shows the speed, output power point, and dynamic performance limit curves of the HSAFPM listed in Table 1 and the HSRFPM listed in Table 2. It can be seen that the dynamic performance limit of the AFPM is ~5 times lower than that of the RFPM. This means that the maximum drive speed range is relatively low compared with the RFPM when using the AFPM topology for the same output power.

6.2. Analysis of the Causes of the Differences in the Dynamic Performance Limit Curves

To analyze the main factor that makes the dynamic performance limit of the AFPM lower than that of the RFPM, additional papers were investigated and analyzed, and it was inferred that the centrifugal force and attractive force are the main factors.

6.2.1. Centrifugal Force

To analyze the centrifugal force effect on the AFPM and RFPM, the hoop stress acting on the retaining ring was calculated. The hoop stress refers to the normal stress acting in the radial direction on the cylinder affected by the internal pressure, and it is expressed by Equation (8) [21]:

$$\sigma_{\theta T} = \frac{3+\nu}{4}\rho_R l_m \omega_m^2 \left[R_{Ro}^2 + \left(\frac{1-\nu}{3+\nu} \right) R_{mo}^2 \right] + P_{ri} \frac{R_{Ro}^2 + R_{mo}^2}{R_{Ro}^2 - R_{mo}^2} \quad (8)$$

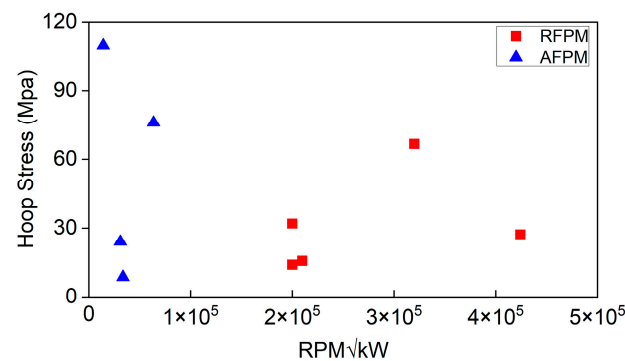
$$P_{ri} = \frac{\rho_m \omega_m^2 (R_{mo}^2 - R_{mi}^2) (R_{mo}^2 + R_{mi}^2)}{4R_{mo}}$$

where ν is Poisson's ratio of the retaining ring, ρ_R is the density of the retaining ring, l_m is the length of the retaining ring, ω_m is the angular velocity of the magnet, R_{Ro} is the outer radius of the retaining ring, R_{mo} is the outer radius of the PM, and P_{ri} is the pressure developed at the inner radius of the retaining ring from the magnet.

The centrifugal force acting on the PM was assumed to be the internal pressure, and the retaining ring was assumed to be the cylinder. In addition, it was assumed that the materials of the PMs and retaining rings of the AFPM and RFPM are all the same. Based on these assumptions, the hoop stresses for the AFPM prototypes listed in Table 1 and the RFPM prototypes listed in Table 2, which provide calculable information, were calculated and shown in Table 3. The magnitude of the hoop stress applied to the PM has various values depending on the linear speed and output power, regardless of the topology. However, if the hoop stress of the machine is plotted against the RPM \sqrt{kW} , as shown in Figure 7, it can be seen that the AFPM receives high hoop stress at a low RPM \sqrt{kW} compared with the RFPM. That is, the AFPM cannot increase the speed at the same output power because the magnitude of the hoop stress according to RPM \sqrt{kW} is larger than that in the RFPM.

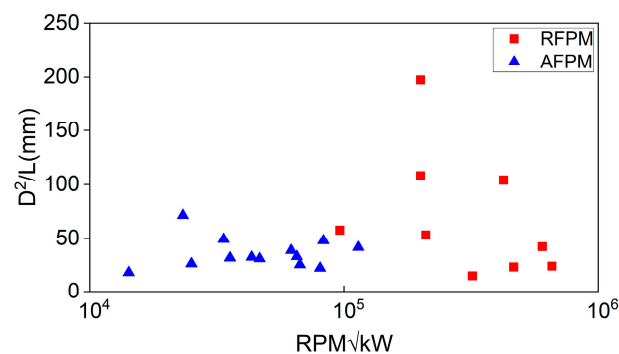
Table 3. Calculation Results of Hoop Stress.

Reference No.	Topology	Power (kW)	N (krpm)	Hoop Stress (MPa)
[28]	AFM	0.1	329.7	110
[10]	AFM	50	188.4	75.9
[23]	RFM	100	147	66.6
[20]	RFM	100	111	32
[25]	RFM	800	160	27.3
[42]	AFM	60	52	24
[22]	RFM	110	91	15.7
[24]	RFM	400	120	14
[38]	AFM	36	64	8.6

**Figure 7.** Hoop stress— $\text{RPM}\sqrt{\text{kW}}$ graph of HSAFPM and HSRFPM.

6.2.2. Windage Loss

The windage loss is the loss due to the air resistance generated when the rotor rotates, and it is proportional to the square of the rotor diameter/axial length (D^2/L) and rotor speed [52]. To compare the windage losses of the AFPM and RFPM, D^2/L was calculated for the $\text{RPM}\sqrt{\text{kW}}$ of the HSAFPM and HSRFPM, as shown in Tables 1 and 3. The calculation results are shown in Figure 8. It can be seen that the AFPM has a similar D^2/L value at a lower $\text{RPM}\sqrt{\text{kW}}$ than the RFPM. This is because the AFPM has a relatively shorter axial length and a larger diameter than the RFPM. Therefore, it can be concluded that at the same speed, a greater windage loss occurs in the AFPM than in the RFPM, resulting in a lower drive speed range.

**Figure 8.** D^2/L — $\text{RPM}\sqrt{\text{kW}}$ graph of HSAFPM and HSRFPM.

6.2.3. Attractive Force

In the RFPM, the attractive force acts in a radial direction. Thus, the PM can be firmly fixed with a retaining ring in the direction of the attractive force, and in the case of an outer rotor type, it can be offset with the centrifugal force to some extent. In other words, the RFPM can use various structural safeguards to avoid problems caused by the

attractive force. However, in the AFPM, since the attractive force acts on the rotor in the axial direction, if a retaining ring is used to protect the permanent magnet, it must be installed in both directions of the attractive force and centrifugal force. Moreover, since the directions of the attractive force and centrifugal force are perpendicular to each other, they do not offset each other out. Therefore, the structural safeguards to prevent problems caused by the attractive force in the AFPM are relatively limited.

7. Conclusions

This paper presents guidelines for determining design specifications when designing AFPM machines as high-speed generators for air vehicles in two steps. Through the literature and product analyses, the key issues to be considered when designing an HSAFPM were described by classifying them as electromagnetic, thermal, and mechanical characteristics, and a dynamic performance limit curve that can estimate the maximum operating speed limit was also presented. By comparing the characteristics of an AFPM and RFPM with the content inferred based on the literature that presented test and evaluation results, it was concluded that the characteristics of the two topologies are inevitably different.

We hope that this paper can be helpful in determining initial design directions when reviewing AFPMs, not only in air vehicles but also in high-speed applications.

Author Contributions: Conceptualization, J.-B.K. and J.-Y.L.; methodology, J.-B.K., J.-H.L. and J.-Y.L.; software, J.-B.K. and J.-Y.L.; validation, J.-B.K. and J.-Y.L.; formal analysis, J.-B.K., J.-H.L. and J.-Y.L.; investigation, J.-B.K. and J.-H.L.; resources, J.-Y.L.; writing—original draft preparation, J.-B.K.; writing—review and editing, J.-Y.L.; visualization, J.-B.K. and J.-Y.L.; supervision, J.-Y.L. All authors have read and agreed to the published version of the manuscript.

Funding: This research was funded by the KERI Primary research program of MSIT/NST, grant number 22A01016.

Institutional Review Board Statement: Not applicable.

Informed Consent Statement: Not applicable.

Data Availability Statement: Not applicable.

Acknowledgments: This research was supported by the Korea Electrotechnology Research Institute (KERI) primary research program through the National Research Council of Science & Technology (NST) and funded by the Ministry of Science and ICT (MSIT) (No. 22A01016).

Conflicts of Interest: The authors declare no conflict of interest.

Nomenclature

AFPM	Axial-flux permanent-magnet machine
R&D	Research and development
RFPM	Radial-flux permanent-magnet machine
SSSR	Single-stator single-rotor
DSSR	Double-stator single-rotor
SSDR	Single-stator double-rotor
HSAFPM	High-speed AFPM
V	Linear speed
r	Rotor radius
N	Rotor's rotational speed
$\text{RPM}\sqrt{kW}$	The figure of merits that evaluates the dynamic performance of machines
P_{core}	Core loss
P_h	Hysteresis loss
K_h	Hysteresis loss coefficient
f	Frequency
B	Flux density amplitude within the material
n	Material-dependent exponent

P_e	Eddy current loss
K_e	Eddy current loss coefficient
P_{em}	Joule loss
PM	Permanent magnet
R_{PM}	The resistance of the eddy current path of the PM
ρ_{PM}	Electrical resistivity of PM
L_{PM}	The length of the eddy current path of PM
A_{PM}	Cross-sectional area of PM
Q_{CD}	Fourier's law of heat conduction
k	Material's conductivity
A_{sur}	Cross-sectional surface area
ΔT	Temperature difference
Δx	The distance
Q_{CV}	Newton's cooling law for convection
h_{cv}	Convection heat transfer coefficient
A_{cont}	Contact area between the solid and fluid
Q_{RA}	Stefan–Boltzmann law for radiation
ε	Emissivity
σ	Stefan's constant
A_{RA}	The radiating area
T_s	Material temperature
T_a	Temperature of the surroundings
AMMs	Amorphous magnetic materials
CFD	Computational fluid dynamics
Dynamic Performance	Speed–output power characteristics
P	Output power
ν	Poisson's ratio
ρ_R	Density of the retaining ring
l_m	The length of the retaining ring
ω_m	The angular velocity of the magnet
R_{ro}	Outer radius of the retaining ring
R_{mo}	Outer radius of PM
P_{ri}	Pressure developed at the inner radius of the retaining ring from the magnet
D	Rotor diameter
L	Rotor axial length

References

1. Cao, W.; Mecrow, B.C.; Atkinson, G.J.; Bennett, J.W.; Atkinson, D.J. Overview of Electric Motor Technologies Used for More Electric Aircraft (MEA). *IEEE Trans. Ind. Electron.* **2012**, *59*, 3523–3531. [[CrossRef](#)]
2. Wang, R.; Tao, S.; Shen, H.; Wang, X.; Li, B.; Shen, G.; Wang, B.; Li, W.; Liu, X.; Huang, Y.; et al. Global Emission of Black Carbon from Motor Vehicles from 1960 to 2006. *Environ. Sci. Technol.* **2012**, *46*, 1278–1284. [[CrossRef](#)] [[PubMed](#)]
3. Emadi, A.; Rajashekara, K.; Williamson, S.; Lukic, S. Topological Overview of Hybrid Electric and Fuel Cell Vehicular Power System Architectures and Configurations. *IEEE Trans. Veh. Technol.* **2005**, *54*, 763–770. [[CrossRef](#)]
4. Gerada, D.; Mebarki, A.; Brown, N.L.; Gerada, C.; Cavagnino, A.; Boglietti, A. High-Speed Electrical Machines: Technologies, Trends, and Developments. *IEEE Trans. Ind. Electron.* **2013**, *61*, 2946–2959. [[CrossRef](#)]
5. Lahne, H.C.; Gerling, D.; Staton, D.; Chong, Y.C. Design of a 50,000 rpm high-speed high-power six-phase PMSM for use in aircraft applications. In Proceedings of the 11th International Conference on Ecological Vehicles and Renewable Energies (EVER), Monte Carlo, Monaco, 6–8 April 2016; pp. 1–11.
6. Varyukhin, A.N.; Ismagilov, F.R.; Vavilov, V.Y.; Ayguzina, V.V.; Gordin, M.V. Design of an electric generator for an aircraft with a hybrid power system. In Proceedings of the 26th International Workshop on Electric Drives: Improvement in Efficiency of Electric Drives (IWED), Moscow, Russia, 30 January–2 February 2019; pp. 1–6. [[CrossRef](#)]
7. Zhang, Z.; Geng, W.; Liu, Y.; Wang, C. Feasibility of a new ironless-stator axial flux permanent magnet machine for aircraft electric propulsion application. *CES Trans. Electr. Mach. Syst.* **2019**, *3*, 30–38. [[CrossRef](#)]

8. Amin, S.; Khan, S.; Bukhari, S.S.H. A Comprehensive Review on Axial Flux Machines and Its Applications. In Proceedings of the 2nd International Conference on Computing, Mathematics and Engineering Technologies (iCoMET), Piscataway, NJ, USA, 30–31 January 2019; pp. 1–7. [[CrossRef](#)]
9. Geng, W.; Zhang, Z. Analysis and Implementation of New Ironless Stator Axial-Flux Permanent Magnet Machine With Concentrated Nonoverlapping Windings. *IEEE Trans. Energy Convers.* **2018**, *33*, 1274–1284. [[CrossRef](#)]
10. Zhang, Z.; Wang, C.; Geng, W. Design and Optimization of Halbach-Array PM Rotor for High-Speed Axial-Flux Permanent Magnet Machine with Ironless Stator. *IEEE Trans. Ind. Electron.* **2020**, *67*, 7269–7279. [[CrossRef](#)]
11. Aydin, M.; Huang, S.; Lipo, T.A. Torque quality and comparison of internal and external rotor axial flux surface-magnet disc machines. In Proceedings of the The 27th Annual Conference of the IEEE Industrial Electronics Society, Denver, CO, USA, 29 November–2 December 2001; pp. 1428–1434.
12. Capponi, F.G.; De Donato, G.; Caricchi, F. Recent Advances in Axial-Flux Permanent-Magnet Machine Technology. *IEEE Trans. Ind. Appl.* **2012**, *48*, 2190–2205. [[CrossRef](#)]
13. Aydin, M.; Huang, S.; Lipo, T.A. Design, Analysis, and Control of a Hybrid Field-Controlled Axial-Flux Permanent-Magnet Motor. *IEEE Trans. Ind. Electron.* **2010**, *57*, 78–87. [[CrossRef](#)]
14. Gieras, J.F.; Wang, R.-J.; Kamper, M.J. *Axial Flux Permanent Magnet Brushless Machines*, 2nd ed.; Springer: Dordrecht, The Netherlands, 2008. [[CrossRef](#)]
15. Lee, J.-Y.; Koo, D.-H.; Moon, S.-R.; Han, C.-K. Design of an Axial Flux Permanent Magnet Generator for a Portable Hand Crank Generating System. *IEEE Trans. Magn.* **2012**, *48*, 2977–2980. [[CrossRef](#)]
16. Lai, J.; Li, J.; Xiao, T. Design of a Compact Axial Flux Permanent Magnet Machine for Hybrid Electric Vehicle. *IEEE Trans. Ind. Electron.* **2021**, *68*, 6630–6639. [[CrossRef](#)]
17. Tenconi, A.; Vaschetto, S.; Vigliani, A. Electrical Machines for High-Speed Applications: Design Considerations and Tradeoffs. *IEEE Trans. Ind. Electron.* **2013**, *61*, 3022–3029. [[CrossRef](#)]
18. Rahman, M.; Chiba, A.; Fukao, T. Super high speed electrical machines—Summary. In Proceedings of the IEEE Power Engineering Society General Meeting, Denver, CO, USA, 6–10 June 2004. [[CrossRef](#)]
19. Li, S.; Li, Y.; Choi, W.; Sarlioglu, B. High-Speed Electric Machines: Challenges and Design Considerations. *IEEE Trans. Transport. Electr.* **2016**, *2*, 2–13. [[CrossRef](#)]
20. Ismagilov, F.R.; Papini, L.; Vavilov, V.E.; Gusakov, D.V. Design and Performance of a High-Speed Permanent Magnet Generator with Amorphous Alloy Magnetic Core for Aerospace Applications. *IEEE Trans. Ind. Electron.* **2020**, *67*, 1750–1758. [[CrossRef](#)]
21. Xu, D.; Wang, X.; Li, G. Design and test for high speed permanent magnet wind generator and research on rotor protection measures. In Proceedings of the 11th IEEE Conference on Industrial Electronics and Applications (ICIEA), Hefei, China, 5–7 June 2016; pp. 2026–2031.
22. Huang, Z.; Fang, J. Multiphysics Design and Optimization of High-Speed Permanent-Magnet Electrical Machines for Air Blower Applications. *IEEE Trans. Ind. Electron.* **2016**, *63*, 2766–2774. [[CrossRef](#)]
23. Zhang, F.; Du, G.; Wang, T.; Liu, G.; Cao, W. Rotor Retaining Sleeve Design for a 1.12-MW High-Speed PM Machine. *IEEE Trans. Ind. Appl.* **2015**, *51*, 3675–3685. [[CrossRef](#)]
24. Jun, H.W.; Park, E.S.; Lee, J.; Lee, H.W. Study on the High Efficiency Design through the Loss Reduction of the 110kW Class High-output Density PMSM. *Trans. Korean Inst. Electr. Eng.* **2015**, *64*, 954–959. [[CrossRef](#)]
25. Jun, H.-W.; Lee, J.; Lee, H.-W.; Kim, W.-H. Study on the Optimal Rotor Retaining Sleeve Structure for the Reduction of Eddy-Current Loss in High-Speed SPMSM. *IEEE Trans. Magn.* **2015**, *51*, 1–4.
26. Du, G.; Huang, N. Multiphysics analysis of high-speed permanent magnet generators for waste heat application. *IET Electr. Power Appl.* **2020**, *14*, 937–942. [[CrossRef](#)]
27. Du, G.; Xu, W.; Zhu, J.; Huang, N. Power Loss and Thermal Analysis for High-Power High-Speed Permanent Magnet Machines. *IEEE Trans. Ind. Electron.* **2020**, *67*, 2722–2733. [[CrossRef](#)]
28. Jang, G.-H.; Ahn, J.-H.; Kim, B.-O.; Lee, D.-H.; Bang, J.-S.; Choi, J.-Y. Design and Characteristic Analysis of a High-Speed Permanent Magnet Synchronous Motor Considering the Mechanical Structure for High-Speed and High-Head Centrifugal Pumps. *IEEE Trans. Magn.* **2018**, *54*, 1–6. [[CrossRef](#)]
29. Hong, D.-K.; Woo, B.-C.; Lee, J.-Y.; Koo, D.-H. Ultra High Speed Motor Supported by Air Foil Bearings for Air Blower Cooling Fuel Cells. *IEEE Trans. Magn.* **2012**, *48*, 871–874. [[CrossRef](#)]
30. Neethu, S.; Fernandes, B.G. Design, analysis and optimization of high speed axial flux permanent magnet synchronous motor for centrifuge application. In Proceedings of the IEEE International Electric Machines & Drives Conference (IEMDC 2017), Miami, FL, USA, 21–24 May 2017; pp. 1–6. [[CrossRef](#)]
31. Phi27 Series. Available online: https://www.phi-power.com/wp-content/uploads/2018/05/Phi271-Spec_Sheet-V1.3.pdf (accessed on 19 March 2022).
32. Phi27x Series. Available online: <https://www.phi-power.com/wp-content/uploads/2017/04/Phi27s-Specsheet-V1.3.pdf> (accessed on 19 March 2022).
33. Phi30 Series. Available online: https://www.phi-power.com/wp-content/uploads/2018/05/Phi301-Spec_Sheet-V1.3.pdf (accessed on 19 March 2022).
34. YASA P400 R Electric Motors Product Sheet. Available online: <https://www.yasa.com/wp-content/uploads/2021/05/YASA-P400RDataSheet-Rev-14.pdf> (accessed on 19 March 2022).

35. Nishanth, F.; Bohach, G.; Van de Ven, J.; Severson, E.L. Design of a Highly Integrated Electric-Hydraulic Machine for Electrifying Off-Highway Vehicles. In Proceedings of the 11th Annual Energy Conversion Congress and Exposition, Baltimore, MD, USA, 29 September–3 October 2019; pp. 3983–3990. [CrossRef]
36. EMRAX 348 Technical Data Table. Available online: https://emrax.com/wp-content/uploads/2020/03/emrax_348_technical_data_table_graphs_5.4.pdf (accessed on 19 March 2022).
37. Wróbel, R.; Vainel, G.; Copeland, C.; Duda, T.; Staton, D.; Mellor, P.; Staton, D. Investigation of mechanical loss and heat transfer in an axial-flux PM machine. In Proceedings of the IEEE Energy Conversion Congress & Expo, Denver, CO, USA, 15–19 September 2013; pp. 4372–4379. [CrossRef]
38. Wang, Z.; Enomoto, Y.; Masaki, R.; Souma, K.; Itabashi, H.; Tanigawa, S. Development of a high speed motor using amorphous metal cores. In Proceedings of the 8th International Conference on Power Electronics & ECCE Asia, Jeju, Korea, 30 May–3 June 2011; pp. 1940–1945. [CrossRef]
39. EMRAX 228 Technical Data Table. Available online: https://emrax.com/wp-content/uploads/2020/03/emrax_228_technical_data_table_graphs_5.4.pdf (accessed on 19 March 2022).
40. Qi, H.; Ling, L.; Liwei, Z. Design and Research of Axial Flux Permanent Magnet Motor for Electric Vehicle. In Proceedings of the 3rd International Electrical and Energy Conference (CIEEC), Beijing, China, 7–9 September 2019; pp. 1918–1923. [CrossRef]
41. EMRAX 188 Technical Data Table. Available online: https://emrax.com/wp-content/uploads/2020/03/emrax_188_technical_data_table_graphs_5.4.pdf (accessed on 19 March 2022).
42. EMRAX 268 Technical Data Table. Available online: https://emrax.com/wp-content/uploads/2020/03/emrax_268_technical_data_table_graphs_5.4.pdf (accessed on 19 March 2022).
43. YASA 750 R Electric Motors Product Sheet. Available online: <https://www.yasa.com/wp-content/uploads/2021/05/YASA-750RDataSheet-Rev-11.pdf> (accessed on 19 March 2022).
44. Le, W.; Lin, M.; Lin, K.; Liu, K.; Jia, L.; Yang, A.; Wang, S. A Novel Stator Cooling Structure for Yokeless and Segmented Armature Axial Flux Machine with Heat Pipe. *Energies* **2021**, *14*, 5717. [CrossRef]
45. Phuong, L.T. Design of Joint Motor for a Collaborative Robot Considering Load and Thermal Characteristics. Ph.D. Thesis, University of Science and Technology, Daejeon, Korea, 2022.
46. Kim, C.-W.; Kim, J.M.; Seo, S.W.; Ahn, J.H.; Hong, K.; Choi, J.Y. Core Loss Analysis of Permanent Magnet Linear Synchronous Generator Considering the 3-D Flux Path. *IEEE Trans. Magn.* **2018**, *54*, 1–4. [CrossRef]
47. Hendershot, J.R.; Miller, T.J.E. Losses and Cooling. In *Design of Brushless Permanent Magnet Machines*, 2nd ed.; Motor Design Books LLC: Venice, FL, USA, 2010; pp. 554–565.
48. Wang, Z.; Enomoto, Y.; Ito, M.; Masaki, R.; Morinaga, S.; Itabashi, H.; Tanigawa, S. Development of a Permanent Magnet Motor Utilizing Amorphous Wound Cores. *IEEE Trans. Magn.* **2010**, *46*, 570–573. [CrossRef]
49. Wang, C.; Qu, R.; Li, J.; Fan, X.; Li, D.; Lu, Y. Rotor loss calculation and thermal analysis of a dual-stator axial-flux permanent magnet machine with combined rectangle-shaped magnets. In Proceedings of the 20th International Conference on Electrical Machines and Systems (ICEMS), Sydney, Australia, 11–14 August 2017; pp. 1–5. [CrossRef]
50. Zhang, B.; Seidler, T.; Dierken, R.; Doppelbauer, M. Development of a Yokeless and Segmented Armature Axial Flux Machine. *IEEE Trans. Ind. Electron.* **2016**, *63*, 2062–2071. [CrossRef]
51. Van Millingen, R.D.; van Millingen, J.D. Phase Shift Torque-meters for Gas Turbine Development and Monitoring. In Proceedings of the International Gas Turbine and Aeroengine Congress and Exposition, Orlando, FL, USA, 3 June 1991; p. V005T15A003.
52. Tong, W. *Mechanical Design of Electric Motors*; CRC Press: Boca Raton, FL, USA, 2014. [CrossRef]